SJIF Impact Factor 2022: 8.197| ISI I.F. Value: 1.241| Journal DOI: 10.36713/epra2016 ISSN: 2455-7838(Online)
EPRA International Journal of Research and Development (IJRD)
Volume: 7 | Issue: 6 | June 2022 - Peer Reviewed Journal

A SERIES RECONFIGURABLE STRUCTURE RESONANT CHOPPER FULLY SOFT-SWITCHED DUAL-ACTIVE-BRIDGE WITH DUAL TANK

[1]C.Selsiya,M.E., [2]Dr.S.Vijayabaskar,M.E., Ph.D., [3]B.Tamilarasi, [4]M.Pavithra, [5]A.Pushparoshini

[1]Assistant Professor, [2]Professor, [3,4,5]UG Students
Department of Electrical and Electronics Engineering
P. A. College of Engineering and Technology, Pollachi, Tamil Nadu, India

Article DOI: https://doi.org/10.36713/epra10462
DOI No: 10.36713/epra10462

ABSTRACT

Compared to the dual-active-bridge converter, the Double - bridge arrangement thunderous converter (DBSRC) can extend delicate- exchanging run. To encourage broaden the soft-switching extend and progress the circuit execution, a modern DBSRC with double tank based on DBSRC is proposed in this paper. This modern converter highlights two thunderous tanks and a tapped transformer, and it can perform superior than the DBSRC by optimized tap coefficient x of the tapped transformer. Its operation guideline, voltage pick up, the soft-switching characteristics, and yield control are analyzed in detail, and compared with the DBSRC. Comes about appear that the pro-posed dual-tank topology has displayed higher voltage pick up, more extensive soft-switching locale, and bigger yield control than the conventional DBSRC when the tap-coefficient x is chosen sensibly. DC-to-DC bidirectional resounding converter to be utilized for bidirectional control exchange applications particularly battery charging/discharging applications in electrical vehicles.

It's similar to an LLC resonant converter, but on the secondary side of the circuit, an additional inductor and capacitor have been added to make the resonant network symmetric for operation in both forward and backward directions. The switches in the inverting step have zero voltage switching (ZVS). Under ZCS, the rectifier diodes on the secondary side also turn off. ZVS and ZCS reduce losses and enable high-frequency operation, resulting in smaller magnetic elements and filter capacitors, lowering size, weight, and volume while enhancing power density.

INDEX TERMS—***dual active bridge (DAB), dual-bridge series resonant converter (DBSRC), soft-switching, dual-tank, tapped-transformer, tap-coefficient***

INTRODUCTION

Bidirectional DC/DC converters possessing improved efficiency and high-power density have been the focus of research in the area of on-board charging/discharging units for electrical vehicles or plug-in electrical vehicles (EV/PHEV). There exists a considerable amount of research work on the isolated bidirectional DC to DC converters. The dual active bridge (DAB) converter topology enjoys great popularity. However, the conventional DAB converter suffers from a few drawbacks. For example, soft switching can be realized for a very narrow output and loading range using the modulation technique of the phase-shifted primary and secondary bridges. To widen the soft switching range of a DAB converter, a number of different DAB control techniques. However, it fails to meet the requirements of the on-board charging/discharging unit voltage range. Moreover, the body diode recovery and turn-off losses of MOSFET switches present a big problem.

Thus, most of the DAB converters employ IGBT switches. Lately much interest has been directed to the area of resonant topologies which offer soft-switching over a wide load range. In particular, the LLC resonant converter has been proposed and studied to increase overall efficiency, since this converter offers soft-switching. However, the LLC resonant converter can transfer power in a unidirectional manner. When operated in the reverse mode, its gain is restricted to below unity. As a novel topology, the CLLC bidirectional resonant converter has been studied and implemented in some energy storage applications. A symmetric LLC-type resonant topology has been put forth for a low-voltage DC power distribution system and high efficiency has been achieved. However, its

SJIF Impact Factor 2022: 8.197| ISI I.F. Value: 1.241| Journal DOI: 10.36713/epra2016 ISSN: 2455-7838(Online)
EPRA International Journal of Research and Development (IJRD)
Volume: 7 | Issue: 6 | June 2022 - Peer Reviewed Journal

voltage range is quite narrow thus it is unfit for use in a EV/PHEV application. A CLLC topology with wide voltage range was proposed and employed in the uninterrupted power supply system with an input/output range of 400V/48V. Nevertheless, in battery charging applications, its transformer ratio is unrealistic because of the considerable difference between the input and output voltages. In this paper, a CLL-LC type bidirectional DC/DC converter to fulfil all the requirements of on-board

EXISTING SYSTEMS

Traditionally, the renewable energy source is connected to the load through a traditional DC-DC converter and then the energy storage system is connected to either the input port or the output port of the traditional DC-DC converter through a bidirectional DC-DC converter. The main disadvantage of these traditional solutions is the low efficiency due to the utilization of the additional converter for the energy storage system. Also, the multi-stage architecture may result in increased size, low power density, and relatively high cost.

Fig. 1 Traditional power electronic systems in renewable energy system

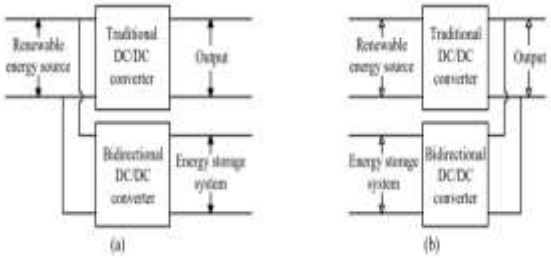

A multi-input converter is a solution to satisfy the requirements of some applications that require the integration of several different types of input energy sources such as fuel cells, wind turbines, and solar PV . This type of converter can be used to provide the demanded power of the load with a single stage technique; however, no energy storage system is included in these multi-input converters, and hence the system may not be able to meet the required load demand when the output power is greater than the input power. For fuel cell operation, this may happen when there is a sudden increase in load and the chemical reaction of the fuel cell is not fast enough to follow the increase in load. Similarly for solar PV application, there may be fast PV output fluctuation during passing cloud causing the PV output to be less than the load demand or when there is no sun irradiation at night. Wind power output also fluctuates with the wind speed variation.

Recently, the three-port DC-DC converters with the configuration shown in Fig. 2 have been studied to integrate the renewable energy and energy storage converters into one converter with two inputs. One three-port DC-DC converter can accept two inputs: one input is for the DC output of the PV, and the second DC input, which is a bidirectional port, is for the energy storage system for charging and discharging. The output of the three-port DC-DC converter can be connected to the DC load directly or to the grid or AC load by an inverter through a DC link capacitor. Many three-port DC-DC converters, which can satisfy the MPPT and energy-storage charging and discharging requirement, have been reported in the literature. These converters can be categorised into 3 types: non-isolated, partly-isolated, and isolated converters. Threeport DC/DC converter Input port bidirectional port Output port .

Non-isolated three-port converters can result in reduced components numbers and a compact structure. Also, a systematic method of the derivation of non-isolated three-port converters. Since all of the three ports are connected directly, this type of converter can only be used in those applications where the galvanic insulation is not required. Another disadvantage of the non-isolated three-port converters is that most of these converters have a limited voltage gain since the freedom of modulation of the voltage conversion ratio is only the duty cycle. Some reported papers use coupled-inductor to extend the voltage conversion ratio to overcome this issue. Compared to the non-isolated three-port converters, partly-isolated three-port converters, which use a transformer to isolate one port from the other two common-grounded ports, can obtain higher voltage gain with a larger turn's ratio of the transformer. However, the energy storage system in these converters continues operating in all operating modes, which can shorten the lifespan of the energy system and lower the reliability of the overall system. Similar to the partly-isolated converters, the isolated converters are based on the use of a high-frequency transformer, which can help them to well balance the different voltage levels among the different ports. However, the number of the components used in this kind of converter is very large since the components are seldom shared. Although both of the partly-isolated and isolated converters can be operated with soft switching on the switches using appropriate control and modulation methods, high power loss may still occur due to the leakage inductance of the transformer. Also, the use of a transformer may make the converter bulky and reduce the overall power density

3.2 PROPOSED SYSTEM

The proposed converter is illustrated in Fig. 4.1. It has a symmetric structure: the primary side circuit resembles the secondary side circuit connected by a symmetric high-frequency transformer. The switches Qi1 … Qi4 in the primary inverting stage convert power from dc to ac to transfer it through the high frequency transformer. Using this transformer, the converter achieves galvanic isolation between the primary side and the secondary side. The leakage inductance of the transformer's primary and secondary windings is incorporated into the resonant inductors Lr1 and Lr2, respectively.

SJIF Impact Factor 2022: 8.197| ISI I.F. Value: 1.241| Journal DOI: 10.36713/epra2016 ISSN: 2455-7838(Online)
EPRA International Journal of Research and Development (IJRD)
Volume: 7 | Issue: 6 | June 2022 - Peer Reviewed Journal

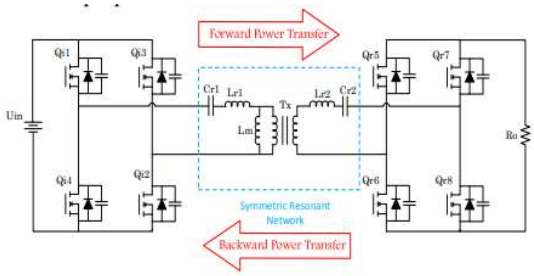

Figure3.3 Schematic of the proposed Converter

3.2.1 Gain analysis through First Harmonic Approximation Model

As the resonant tank works like a bandpass filter, commonly it is assumed that power transfer takes place mainly through the fundamental components of the voltages and currents. This is called the first harmonic approximation (FHA). In that sense, the square-wave applied to the resonant tank is represented by its fundamental component. From Fig. 4.1, the converter electrical circuit can be simplified to develop an expression for the gain of the resonant network in terms of switching frequency. The input voltage of the network, uri, is a square waveform which varies from −Uin to Uin. Using the Fourier series, it can be expressed as follows:

$$u_{ri}(t)=\frac{4U_{in}}{\pi}\sum_{n=1,3,5,\ldots}^{\infty}\frac{1}{n}\sin(2\pi n f_s t) \qquad (1)$$

where t is the time parameter, n is the integer parameter for the Fourier series expansion, and fs is the switching frequency of the inverting stage switches, respectively.

The fundamental component of uri, uri,FHA, can be extracted from (1) using the FHA method as shown in the following equation:

$$U_{ri,FHA}=\frac{2\sqrt{2}}{p}U_{in} \qquad (3)$$

The rms value of uri,FHA, Uri,FHA, can be calculated as

In the same way, the output voltage of the resonant network, uro, can be expressed as follows:

$$u_{ro}(t)=\frac{4U_o}{\pi}\sum_{n=1,3,5,\ldots}^{\infty}\frac{1}{n}\sin(2\pi n f_s t-\phi) \qquad (4)$$

Where φ is the phase shift with respect to the input voltage. Then, the fundamental component of uro , FHA, can be extracted from (4) as follows:

$$u_{ro,FHA}(t)=\frac{4}{\pi}U_o\sin(2\pi f_s t-\phi) \qquad (5)$$

The RMS value of euro ,FHA, Uro, FHA, can be calculated

The fundamental component of the rectifier current irct, irct,FHA can also be expressed in the same manner as (2) and (5) as follows:

$$U_{in,FHA}=\frac{2\sqrt{2}}{\pi}U_o \qquad (6)$$

Where Irct, FHA is the RMS value of irct,FHA. Therefore, the average output current Io can be derived using (7) as follows:

$$i_{rct,FHA}(t)=\sqrt{2}I_{rct,FHA}\sin(2\pi f_s t-\phi) \qquad (7)$$

$$I_o=\frac{2}{T_s}\int_0^{\frac{T_s}{2}}\left|i_{rct,FHA}(t)\right|dt=2\sqrt{2}I_{rct,FHA} \qquad (8)$$

Since uro, FHA and irct, FHA are in phase, the resistive load of the resonant network, Ro,e, is equal to the ratio of the instantaneous voltage and current as shown in (9) with the load resistance, Ro

$$R_{o,e}=\frac{U_{ro,FHA}}{I_{rct,FHA}}=\frac{8}{\pi^2}R_o \qquad (9)$$

$$M_F=\frac{1}{n}\left|\frac{R_{o,e}}{R_{o,e}+Z'_{Lr2}+Z'_{Cr2}}\frac{(R_{o,e}+Z'_{Lr2}+Z'_{Cr2})//Z_{Lm}}{Z_{Lr1}+Z_{Cr1}+(R_{o,e}+Z'_{Lr2}+Z'_{Cr2})//Z_{Lm}}\right| \qquad (10)$$

$$M_B=\frac{1}{n}\left|\frac{R_{o,e}}{R_{o,e}+Z'_{Lr1}+Z'_{Cr1}}\frac{(R_{o,e}+Z'_{Lr1}+Z'_{Cr1})//Z_{Lm}}{Z_{Lr2}+Z_{Cr2}+(R_{o,e}+Z'_{Lr1}+Z'_{Cr1})//Z_{Lm}}\right| \qquad (11)$$

Based on the approach of fundamental harmonic approximation, the equations of the dc gain for both forward power transfer mode and backward power transfer mode can be expressed as follows.

$$R_{o,e}=(8n^2/\pi^2)R_o \qquad L'_{r2}=n^2\cdot L_{r2}$$
$$C'_{r2}=\frac{C_{r2}}{n^2}$$

Where MF and MB are the forward and backward mode gains respectively and,the gain curves with respect to load current and normalized frequency, which is derived using (10). The peak value of the gain occurs at the low resonant frequency which includes the magnetizing inductance as a resonant component. At the series resonant frequency (without Lm), the converter's gain is slightly higher than unity. Under light-load conditions, the converter has a high gain and the gain curve is steep. However, the overall value of the gain curve decreases under the heavy-load condition. A higher load results in the lower gain in the bidirectional CLL-LC resonant converter.

SJIF Impact Factor 2022: 8.197| ISI I.F. Value: 1.241| Journal DOI: 10.36713/epra2016 ISSN: 2455-7838(Online)
EPRA International Journal of Research and Development (IJRD)
Volume: 7 | Issue: 6 | June 2022 - Peer Reviewed Journal

3.3 CIRCUIT DIAGRAM

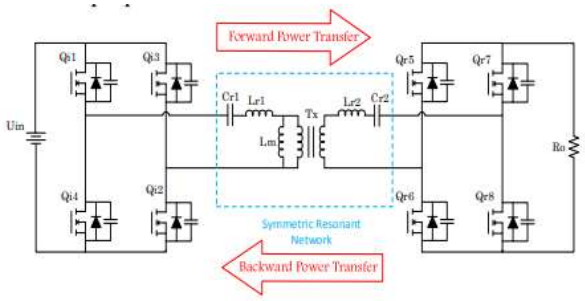

Figure 3.4 Circuit diagram

Then different operational intervals of the proposed bidirectional CLL-LC resonant converter. This converter's operation has been divided into eight operational intervals during a single switching cycle. Intervals 1, 2, 3 and 4 repeat to intervals 4, 5, 6 and 7 with different inverting and rectifying switch pairs. Intervals 2,3 and 4 are dead-time durations, intervals 1 and 5 are power transfer modes. The primary switches work in the inverting mode when power is transferred from the primary to the secondary side; however, the secondary switches remain OFF and the antiparallel diodes operate as rectifiers on the secondary side. Error! Reference source not found. gives theoretical waveforms showing the behavior of the converter for all intervals during a single switching cycle. In Error! Reference source not found., there are only the waveforms of the charging mode. However, in the discharging mode, the waveforms are precisely the same as the waveforms of the charging mode, because the primary inverting side and the secondary rectifying side are symmetric. Detailed explanation and description of the operational intervals are given below: Interval 1 [t0 ,t1]: At the instant t0 , the switches Qi1 and Qi2 are conducting and power is transferred from the primary stage to the secondary stage. Resonance takes place between the series elements Cr1, Lr1, Lr2 and Cr2, and the resonant current iLr1 rises in a sine-wave curve. The current in magnetizing inductor iLm also increases but resonates considerably slower than iLr1. Thus Lm does not take part in the resonance phenomenon in this interval. On the secondary side, the rectified currents iQr6 and iQr7, which are carried by the anti-parallel diodes of Qr6 and Qr7 , are proportional to the difference between the terms iLr1and iLm. Interval 2 [t1 ,t2]: After attaining its peak value, iLr1 begins to decline and at the instant t1 becomes equal to the slowly rising magnetic current iLm. The rectifier current on the secondary side decreases to zero, and the anti-parallel diodes of Qr6 &Qr7 turn off under ZCS. The voltage on the resonant capacitor Cr2 also resonates to its peak with the absolute value of VCr2. It will remain unchanged unless it excites again in the next resonance. The free resonance between Cr1, Lr1, and Lm on the primary side is availed by the disconnection of Cr2 and Lr2. Interval 3 [t2 ,t3]:At time t2 , Qi1 and Qi2 turn off. iLr1 begins to charge the parasitic capacitance of Qi1 and Qi2, and discharge that of Qi3 and Qi4 simultaneously. Since the value of the parasitic capacitance is small compared with that of the resonant capacitor Cr1, this time period is rather short with respect to the total switching period. Thus, the corresponding voltages on the aforementioned capacitance rise/decrease rapidly. This stage ends up with vdQi1,2 reaching the input voltage and vdQi3,4 decreasing to zero. At the end of this stage, the voltage applied on the resonant tank has changed polarity from positive Uin to negative. Interval 4 [t3 ,t4]: When Qi3 and Qi4 are completely discharged, the resonant current iLr1 immediately starts flowing through the anti-parallel body diodes of Qi3 and Qi4, and is fed back to the input source. When the voltage of the magnetic inductor Lm resonates to reach the voltage of V2 –VCr2, the rectifier switches Qr5 and Qr8 conduct, and the resonant capacitor Cr2 and Lr2 participate the resonance with the primary side again. At time t4 , Qi3 and Qi4 turn on under ZVS conditions, the first-half switching period ends, and the converter enters the next (the second) half.

3.4 BLOCK DIAGRAM

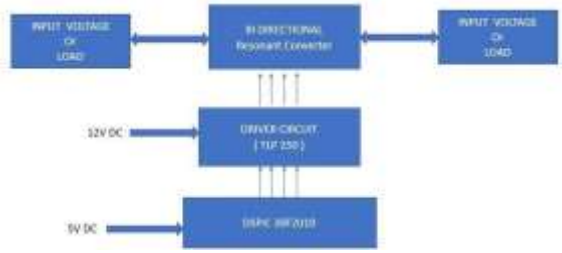

Figure 3.6 Block Diagram

You can switch the input pulses initially given to the low voltage side and convert them to the high voltage side. This switch inputs the pulses applied to the inverter by Q1, Q2, Q3, and Q4. These are symmetric in nature and maintain high frequencies. ZVS, ZCS operation reduces switching losses and frequency coupled choke coil or transformer. Frequency can hold above 25kHz. The driver circuit is used to regulate the current through the circuit and to control other factors such as other components and some devices in the circuit. H bridge diode can be act as a rectifier and connected to load R. Here L is resonant frequency transformer and c is a capacitance.

MATLAB IMPLEMENTATION

5.1 MATLAB SIMULATION & RESULTS

MATLAB is the high-level language and interactive environment used by millions of engineers and scientists worldwide. It lets you visualize ideas disciplines including signals and image processing, communications, control systems, and computational finance. In SIMULINK, it is very straight forward to represent and then simulate a mathematical model representing a physical system. Models are represented graphically in SIMULINK as block diagrams. A wide array of

SJIF Impact Factor 2022: 8.197| ISI I.F. Value: 1.241| Journal DOI: 10.36713/epra2016 ISSN: 2455-7838(Online)
EPRA International Journal of Research and Development (IJRD)
Volume: 7 | Issue: 6 | June 2022 - Peer Reviewed Journal

blocks are available to the user in provided libraries for representing various phenomena and models in a range of formats. One of the primary advantages of employing SIMULINK (and simulation in general) for the analysis of dynamic systems is that it allows us to quickly analyse the response of complicated systems that may be prohibitively difficult to analyse analytically. SIMULINK is able to numerically approximate the solutions to mathematical models that we are unable to, or don't wish to, solve "by hand." In general, the mathematical equations representing a given system serve as the basis for a SIMULINK model can be derived from physical laws.

5.2 INTRODUCTION TO SIMULINK

SIMULINK is a software add-on to mat lab which is a mathematical tool developed by The Math works,(http://www.mathworks.com) a company based in Natick. MATLAB is powered by extensive numerical analysis capability. Simulink is a tool used to visually program a dynamic system (those governed by Differential equations) and look at results. Various toolboxes for different techniques, such as Fuzzy Logic, Neural Networks, DSP, Statistics etc. are available with SIMULINK which enhance the processing power of the tool. The main advantage is the availability of templates building blocks, which avoid the necessity of typing code for small mathematical processes.

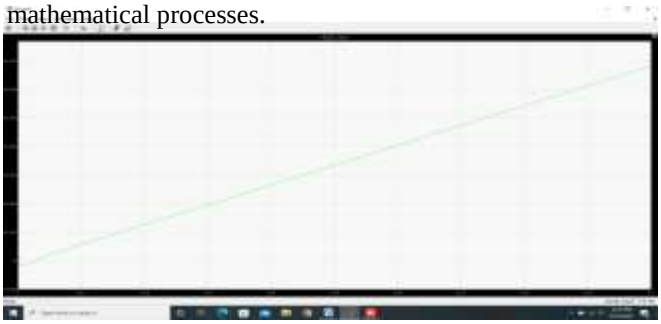

Figure 5.1 Dual bridge series resonant dc to dc converter simulink diagram

5.3 RESULTS

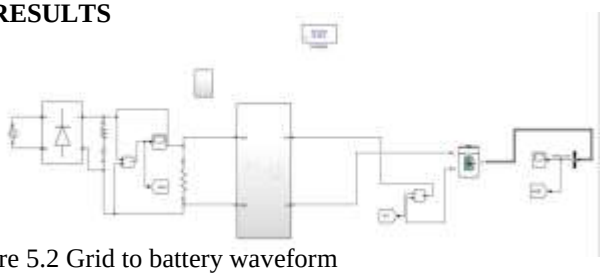

Figure 5.2 Grid to battery waveform

Figure 5.4 Input bridge rectifier dc voltage waveform

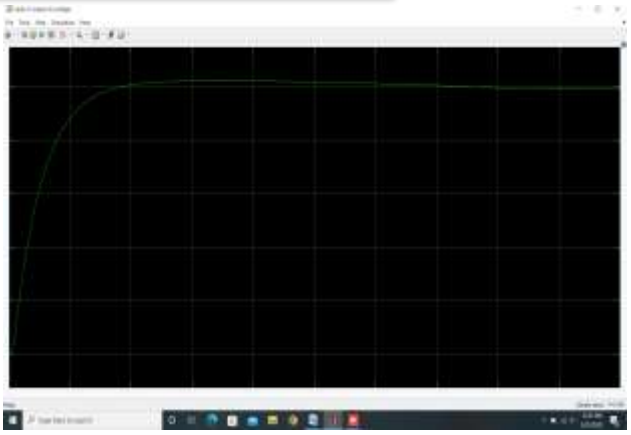

Figure 5.5 Battery discharging waveform

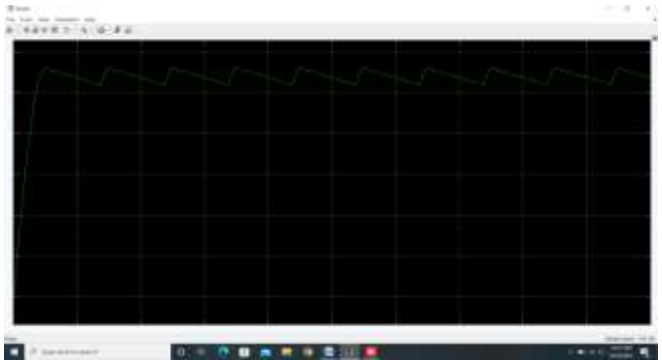

Figure5.6 Battery charging waveform

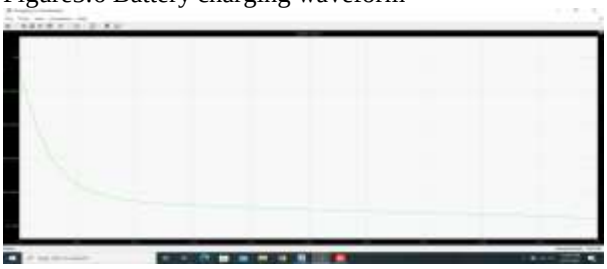

HARDWARE PHOTOGRAPHY

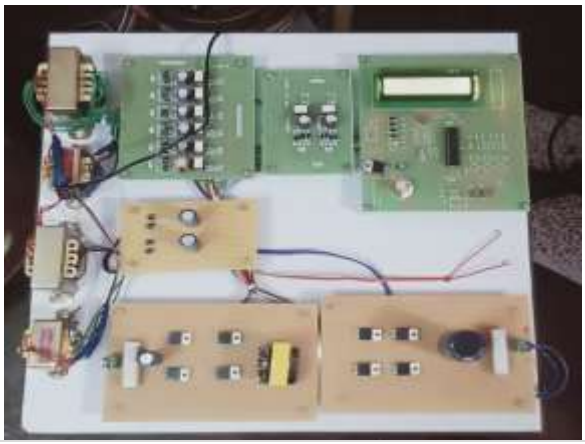

SJIF Impact Factor 2022: 8.197| ISI I.F. Value: 1.241| Journal DOI: 10.36713/epra2016 ISSN: 2455-7838(Online)
EPRA International Journal of Research and Development (IJRD)
Volume: 7 | Issue: 6 | June 2022 - Peer Reviewed Journal

The CLL-LC bidirectional DC-DC converter presented in this paper, which has a symmetric resonant tank, offers soft switching as zero voltage switching for the inverting stage and zero current switching for the rectifier switches irrespective of the direction of flow of power. Thus, when MOSFETs are employed as the main switches, the converter has decreased switching losses and is totally snubber less offering reduced size, weight and volume. The operation principles and simulations of the proposed converter have been analysed and depicted. It has been shown that the simulated converter exhibits ZVS for the inverting stage and ZCS for the rectifying stage. The simulation results validate the theoretical analysis and the merits of the converter. Keeping this in view, the converter offers itself as an alternative choice with wide input range, improved efficiency, and high-power density particularly suited for on-board battery charging/discharging applications in electrical vehicles.

REFERENCES

1. *Mummadi Veerachary ; Vasudha Khubchandani, Year: 2019, "Analysis, Design, and Control of Switching Capacitor Based Buck–Boost Converter", IEEE Transactions on Industry Applications, vol. 55, no. 3, pp. 2845 – 2857.*
2. *Ki-Duk Kim ; Hyung-Min Lee ; Sung-Wan Hong ; Gyu-Hyeong Cho, Year: 2019, "A Noninverting Buck–Boost Converter With State-Based Current Control for Li-ion Battery Management in Mobile Applications", IEEE Transactions on Industrial Electronics, pp. 66, no. 12, pp. 9623 – 9627.*
3. *Hongfei Wu ; Tiantian Mu ; Hongjuan Ge ; Yan Xing, Year: 2016, "Full-Range Soft-Switching-Isolated Buck-Boost Converters With Integrated Interleaved Boost Converter and Phase-Shifted Control", IEEE Transactions on Power Electronics, vol. 31, no. 2, pp. 987 – 999.*
4. *Abdul Hakeem Memon ; Mazhar Hussain Baloach ; Anwar Ali Sahito, Year: 2018, "Achieving High Input PF for CRM Buck-Buck/Boost PFC Converter", IEEE Access, vol. 6, pp. 227 – 240.*
5. *Yangjun Lu ; Hongfei Wu ; Kai Sun ; Yan Xing, Year: 2016, "A Family of Isolated Buck-Boost Converters Based on Semiactive Rectifiers for High-Output Voltage Applications", IEEE Transactions on Power Electronics, vol. 31, no. 9, pp. 6327 – 6340.*
6. *Hai Young Jung ; Sung Hwan Kim ; Byunghee Moon ; Seok-Hyun Lee, Year: 2018, "A New Circuit Design of Two-Switch Buck-Boost Converter", IEEE Access, vol. 6, pp. 47415 – 47423.*
7. *Mohamed O. Badawy ; Yilmaz Sozer ; J. Alexis De Abreu-Garcia, Year: 2016, "A Novel Control for a Cascaded Buck–Boost PFC Converter Operating in Discontinuous Capacitor Voltage Mode", IEEE Transactions on Industrial Electronics, vol. 63, no. 7, pp. 4198 – 4210.*
8. *Erfan Maali ; Behrooz Vahidi, Year: 2016, "Double-Deck Buck-Boost Converter With Soft Switching Operation", IEEE Transactions on Power Electronics, vol. 31, no. 6, pp. 4324 – 4330.*
9. *Leonardo Callegaro ; Mihai Ciobotaru ; Daniel J. Pagano ; Eugenio Turano ; John E. Fletcher, Year: 2018, "A Simple Smooth Transition Technique for the Noninverting Buck–Boost Converter", IEEE Transactions on Power Electronics, vol. 33, no. 6, pp. 4906 – 4915.*
10. *Niraj Rana ; Arnab Ghosh ; Subrata Banerjee, Year: 2018, "Development of an Improved Tristate Buck–Boost Converter With Optimized Type-3 Controller"IEEE Journal of Emerging and Selected Topics in Power Electronics, vol. 6, no. 1, pp. 400 – 415.*
11. *Majid Abbasi ; Ahmad Afifi ; Mohamad Reza Alizadeh Pahlavani, Year: 2019, "Comments on "A Single-Inductor Multiple-Output Switcher With Simultaneous Buck, Boost, and Inverted Outputs", IEEE Transactions on Power Electronics, vol. 34, no. 2, pp. 1980 – 1984.*
12. *Benfei Wang ; Xinan Zhang ; Jian Ye ; Hoay Beng Gooi, Year: 2019, "Deadbeat Control for a Single-Inductor Multiple-Input Multiple-Output DC–DC Converter", IEEE Transactions on Power Electronics, vol. 34, no. 2, pp. 1914 – 1924.*
13. *Daniel Thenathayalan ; Joung-Hu Park, Year: 2018, "An Independently Controlled Single-PWM Multiple-Output Narrow-Band Resonant Converter", IEEE Transactions on Power Electronics, vol. 33, no. 6, pp. 5042 – 5061.*
14. *Guipeng Chen ; Yan Deng ; Jie Dong ; Yihua Hu ; Lin Jiang ; Xiangning He, Year: 2017, "Integrated Multiple-Output Synchronous Buck Converter for Electric Vehicle Power Supply", IEEE Transactions on Vehicular Technology, vol. 66, no. 7, pp. 5752 – 5761.*